Design and Analysis of AFPM Coreless Motor for Electric Scooter

Chul-Ho Kim* and Chul-Soo Oh**

Abstract - This paper deals with the design and the characteristic analysis of a coreless axial flux permanent magnet (AFPM) motor. Because a direct-drive wheel motor is easily derived from it, the AFPM motor is very suitable for application in an electric scooter. Compared to a conventional motor of the same size and weight, the AFPM motor is proven to have more power and torque per unit weight. In this paper, an AFPM coreless motor with a double-sided rotor disk equipped with Nd-Fe-B rare earth magnets is designed and a prototype of the motor is manufactured, which will be properly applied for the low-speed, and high-torque direct drive required for the electric scooter. The manufactured prototype of the motor has a rating of 300W, 510rpm, 5.6Nm, and 85% efficiency.

Keywords: AFPM coreless motor, electric scooter, brushless permanent magnet motor

1. Introduction

Motors can be classified as radial flux or axial flux, depending on the flux path interacting with torque generation. The axial flux motor has an airgap surface vertical to its shaft axis, and magnetic flux interacting with the torque generation of the conductor coil is directed to the axial direction. Generally, the axial flux permanent magnet (AFPM) motor has a higher energy density due to its structural advantage; the path of the magnetic flux is relatively short compared with that of the radial flux type motor. Secondly, the AFPM motor has a large radius for torque production.

The AFPM motor has been proven to be most suitable for low-speed and high-torque applications. This means that the motor can easily be equipped with a multi-pole permanent magnet, resulting in a disk-like motor shape. Such design is well suited to the wheels, the mechanical structure of the electric scooter, and a direct-drive wheel motor is easily derived. Compared to conventional motors of the same size and weight, the AFPM motor is proven to have a higher power rating [1,2]. Thus, the AFPM motor has a higher value of power and torque per unit weight and motor efficiency.

In the general construction configuration of an AFPM motor, the stator with exciting coils is located in the middle of the motor and rotor with permanent magnets is present on both sides of the stator. Another configuration that can exist contains the rotor with permanent magnets is located in the middle of the machine and stator with exciting coils is attached on both sides.

Z. Zhang has classified AFPM to core and coreless types, depending on the stator structure. The core type can be further classified into slot and slotless types. The AFPM motor can be classified as surface-mounted PM and interior-mounted PM types depending on the mounting of the permanent magnets [3]. The model introduced by Spooner is a torus AFPM motor with a core and a surface-mounted magnet [4]. In torus type of AFPM motor, the magnet N pole is facing the N pole in opposite side of the rotor. Magnetic flux from one pole is returned to the adjacent poles of the same disk through the stator core.

The AFPM machine operates in brushless status with position sensor, and its torque characteristic is similar to that of the brushless DC motor. Therefore, all AFPM motors are understood as brushless DC motors, and today's AFPM brushless DC motor has a higher energy efficiency and a higher ratio of energy density per unit active volume than induction motors or direct current motors [5-9]. Development of the rare earth permanent magnet (Nd-Fe-B), which has a high energy density, widens the application of the AFPM motor [10].

In this paper, the AFPM motor chosen has a coreless stator and a double-sided rotor with surface-mounted permanent magnet. A prototype of this motor is manufactured, and will be used for low-speed, high-torque applications such as an electric scooter. Output power and efficiency in the low-speed region show good results. Theoretical study and the testing will determine the possibility of the electric scooter application.

2. AFPM Coreless Motor

2.1 Structure of the AFPM Motor

The AFPM motor has a brushless structure. The coreless

* Dept. of Electrical Engineering, Graduate School of Kyungpook National University, Korea (ch8kim@hanmail.net).
** School of Electrical Engineering and Computer Science, Kyung-pook National University, Korea (csoh@knu.ac.kr).
Received March 4, 2003 ; Accepted April 10, 2003

stator is equipped with three phase coils, driven by the inverter, which triggers the switch according to the pos ition of the rotor magnet. The rotor consists of a doubl -sided iron disk, equipped with Nd-Fe-B rare earth magnets in both sides. In the prototype of this machine, the number of the pole of magnets is selected as 20 and the outer diameter is 208 mm. A yoke ring supports two disks in transversa direction and serves as a coupling for the magnetic poles of the rotor. The AFPM motor needs a rotor position information and commutating process with stator coil exciting. A Hall effect sensor or photo effect sensor could b used for detecting the rotor position, and in this research a photo sensor is adopted. Fig.1 is the half-section view of the AFPM motor.

The magnet N pole is facing the S pole in the opposit side of the rotor so that magnet flux is interacting with the exciting coil purely in axial direction. The magnetic path has a loop form of circuit starting from the half side of N to another half side of S, going to beneath N via rotor steel plate, arriving to S as shown in Fig. 2. The magnetic flux in the airgap depends on the material of the permanent magnet, the thickness of the permanent magnet, and the airgap length.

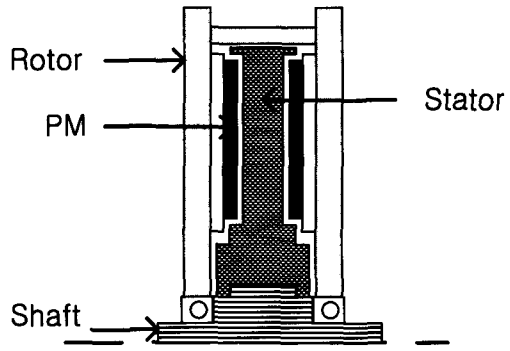

Fig.1 Basic structure of the coreless AFPM motor

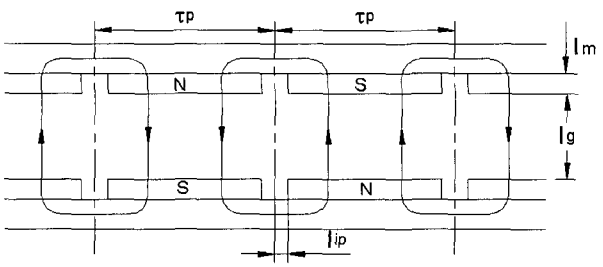

Fig. 2 Magnetic flux path

2.2 Airgap Magnetic Flux Simulation

For the purpose of finite element simulation, a 2-D model of the AFPM motor of Fig. 2 is used. In this model, inter-pole gap, l_{ip}, is introduced to find the effect of magnetic flux leakage. As shown in Fig.3, which simulates the prototype AFPM moto 's section in a two-dimensional, finite element method (FEM) way, the magnetic flux has an axis symmetry pattern. So explaining only one path of the magnetic flux makes it possible to understand the entire magnetic circuit. Through this simulation, leakage flux that fails to cross the stato 's conductor and that could not f-fect the effective torque can be detected.

Shown in Fig. 4 is the axial magnetic flux density of th motor on the circumference of the representative radius at the airgap in variation of interval ratio α, which is defined as the interval ratio of the inter-pole gap, l_{ip}, to pole pitch, τ_p. According to the result, an interval ratio of 4% is chosen for a prototype motor. The two dimensional finite element analysis program used in this simulation is Maxwell 2D from Ansoft.

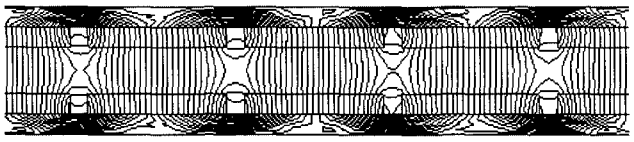

Fig. 3 Distribution of flux density

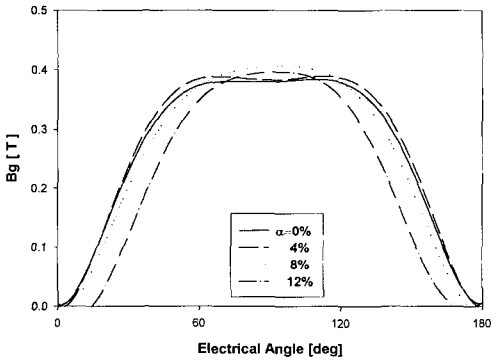

Fig. 4 Airgap flux density in variation of interval ratio

2.3 AFPM Moto 's Characteristic Equation

The section view of the AFPM motor along to circle with middle diameter of machine with exciting coil is shown in Fig. 5. The three-phase exciting coils exist, but only one phase coil is shown in Fig 5. The total number of coil turns in the stator, N, is expressed as

$$N = 3\frac{p}{2}N_{ph} \tag{1}$$

where N_{ph} is the number of coil turns per pole per phase.

The equivalent magnet circuit model along one magneti path in Fig. 2 is shown in Fig. 6. Magnetic flux density at the airgap is expressed as

$$B_g = \frac{\phi_g}{A_g} = \frac{4F_m}{\frac{A_g}{2}(8R_m + 4R_g + 2R_c)} \quad (2)$$

where ϕ_g is airgap magnetic flux, A_g is airgap area, F_m is magnetomotive force of permanent magnet, R_m is reluctance of magnet, R_g is reluctance of airgap, and R_c is reluctance of back iron per pole length τ_p.

Magnetomotive force of the permanent magnet can be expressed using residual flux density B_r, thickness l_m and permeability μ_m.

$$F_m = \frac{B_r l_m}{\mu_m} \quad (3)$$

Neglecting the reluctance of back iron R_c, (2) becomes

$$B_g = \frac{B_r}{1 + \frac{\mu_r l_g}{2 l_m}} \quad (4)$$

where μ_r is recoil permeability of the magnet and l_g is airgap length.

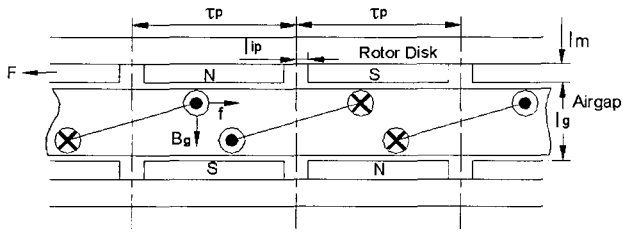

Fig. 5 Configuration of stator coils demonstrating one phase serial coils

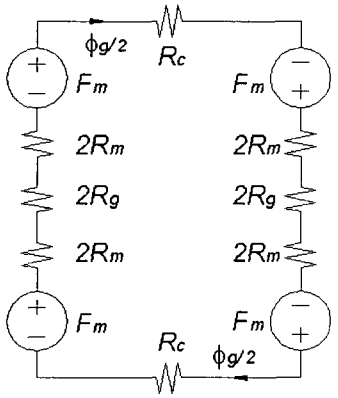

Fig. 6 Equivalent magnetic circuit of the motor

Spooner gives the general torque equation of the AFPM motor as per (5). His machine has a ring core with torus winding, and magnetic flux from the rotors are directing to the ferro-material core in a concentric direction because the magnet N pole is facing the N pole in the opposite side of the rotor directed in both side.

The AFPM motor's torque is formed by interaction with the magnetic flux of the airgap created by the permanent magnet and the electric loading, J_i, in the stator inner radius from the current that flows in the stator winding. So the total torque created from each side of the stators can be expressed as

$$T = 2\pi B_g J_i R_i (R_o^2 - R_i^2) \quad (5)$$

where B_g is airgap magnetic flux density, R_o is outer radius of stator winding, R_i is inner radius of stator winding, and J_i is electric loading along with the line of radius circle with radius R_i [4]. Because one direction of magnetic flux is functioning, (5) will be modified in our AFPM motor as follows.

$$T = \pi B_g J_i R_i (R_o^2 - R_i^2) \quad (6)$$

First, we need to formulate this equation with our known factors: number of poles p, number of coil turns per pole-pair per phase N_{ph}, current in coil per phase I_{1eff}, maximum value of magnetic flux per pole $\hat{\phi}_m$, and total coupling area of magnetic flux for one phase coil A. To do that, we have to modify the equation as follows.

$$\begin{aligned} T &= B_g J R_{rp} A \\ &= \frac{p^2}{2\pi} B_g J \frac{2\pi R_{rp}}{p} A_p \end{aligned} \quad (7)$$

where J is electric loading along with the circumference of the representative radius R_{rp}, A_p is the coupling area of magnetic flux per pole for one phase coil, and ($B_g A_p$) can be stipulated to ($\frac{\hat{\phi}_m}{\sqrt{2}} k_\phi$).

$$J = \frac{2NI}{2\pi R_{rp}} = \frac{2N_{ph}}{2\pi R_{rp}/p} 1.5 I_{1eff} \quad (8)$$

From (7) and (8),

$$T = \frac{1.5}{\sqrt{2}\pi} p^2 (N_{ph} I_{1eff})(\hat{\phi}_m k_\phi) \tag{9}$$

where $\hat{\phi}_m$ is maximum magnetic flux per pole and k_ϕ is coefficient of magnetic flux distribution.

Secondly, the torque equation of the motor from the concept of energy conversion can be derived as follows. In a system with a coil in which current, i, with self inductance, L, is mutually coupled with a permanent magnet with mutual flux, ϕ_m, and reluctance, R, the torque of the system can be formulated as follows [11,12]:

$$T(\theta) = \frac{1}{2} i^2 \frac{dL}{d\theta} - \frac{1}{2} \phi_m{}^2 \frac{dR}{d\theta} + Ni \frac{d\phi_m}{d\theta} \tag{10}$$

In this expression, the first two terms are reluctance torque associated with the coil and magnet, respectively, and the third is the alignment torque due to the mutual flux linking the magnet to the coil. The second term is torque component proportional to the square of the flux leaving the magnet and is not a function of the polarity of the flux. The minus sign occurs in front of this term because inductance is inversely proportional to reluctance.

In our AFPM motor, the differentiation of self-inductance of the coil by increasing the distance angle is 0 due to disks in both sides and the differentiation of reluctance of the permanent magnet by increasing the distance angle is 0 because the stator has no core. So only the last term of the equation (10) remains.

$$T(\theta) = Ni \frac{d\phi_m}{d\theta} = (\frac{p}{2} N_{ph}) i (p \frac{d\phi_m}{d\theta}) \tag{11}$$

Assuming the current is sinusoidal and the magnetic flux is square wave,

$$\begin{aligned} T &= \frac{p^2}{2} N_{ph} (\frac{1.5}{\sqrt{2}} I_{1eff})(\hat{\phi}_m k_\phi) \frac{1}{2} \times \frac{4}{\pi} \\ &= \frac{1.5}{\sqrt{2}\pi} p^2 (N_{ph} I_{1eff})(\hat{\phi}_m k_\phi) \end{aligned} \tag{12}$$

Finally, the two torque equations, (9) and (12), derived from the both concepts of the view, i.e., from Lorentz force law and energy conversion law, are identical.

Copper loss, P_C, at the stator coils makes a significant contribution to the total loss because this AFPM motor is coreless. The heat from the copper loss is eliminated at the airgap, between the stator and the rotor, through the flow of the air. Spooner depicts the copper loss as [4]

$$P_C = \frac{C_J I_{1eff}^2}{d^2} \tag{13}$$

where d is the diameter of the conductor and C_J is constant and expressed as follows.

$$C_J = \frac{m k_w 4 p \rho_o N_{ph} (R_o - R_i)}{\pi a} \tag{14}$$

where m is the number of phases, k_w is winding coefficient, ρ_0 is resistivity of copper, and a is number of parallel circuits.

2.4 Practical Calculation

The prototype motor has the following parameters.

$$\begin{aligned} p &= 20, \\ N_{ph} &= 16, \\ I_{1eff} &= 8.4A \end{aligned}$$

From (4), the airgap flux density is

$$B_g = \frac{1.25}{1 + \frac{1.05 \times 13}{2 \times 3}} = 0.38T$$

and the effective flux per pole is

$$\begin{aligned} \phi_m k_\phi &= \frac{0.38 \times \pi (0.10^2 - 0.06^2) \times 0.85}{20} \\ &= 0.35mWb. \end{aligned}$$

From (9), torque is calculated as

$$T = \frac{1.5}{\sqrt{2}\pi} \times 20^2 (16 \times 8.4)(0.35 \times 10^{-3}) = 6.4Nm.$$

From (8), electric loading at the representative radius is

$$J = \frac{2 \times 16}{2\pi \times 0.085/20} 1.5 \times 8.4 = 15.1kA/m.$$

From (14), coefficient C_J is

$$\begin{aligned} C_J &= \frac{3 \times 2 \times 4 \times 20 \times 1.72 \times 10^{-8} \times 16 (0.10 - 0.06)}{2\pi} \\ &= 0.88 \times 10^{-6} \Omega m^2. \end{aligned}$$

Copper loss is

$$P_C = \frac{0.88\times10^{-6}\times8.4^2}{(1.2\times10^{-3})^2} = 43W .$$

Efficiency considering only copper loss can be expressed as

$$\eta = \frac{300}{300+43} = 87.5\% .$$

The calculated value of torque is a little larger than the rated value, 5.6Nm. Equation (9) can be used for the practical prediction of the prototype motor. Also, copper loss and efficiency considering only its loss are properly calculated.

2.5 Experimental Results

A prototype AFPM motor has mechanical and electrical parameters as shown in Tables 1 and 2. The motor is coreless and consists of disc shape rotors. The ratio of outside to inside radius of the motor is 1.7, which is very close to $\sqrt{3}$ to obtain theoretical maximum torque density [5]. The rotor and stator are pictured in Figs. 7 and 8. The reflecting magazine is equipped for a position sensor at the rotor, and the photo sensor is located at the stator for driving the gate of inverter.

The driving inverter system consists of a voltage-type PWM inverter. Fig. 9 shows the waveform of the phase electromotive force and load current at the rated speed. The ideal waveforms of sinusoidal EMF and six-step driving current are shown for comparison with the experimental waveforms. The experimental waveform of EMF is measured at the generating mode of the rated speed. The FEM simulation result of the flux density of the airgap at the α=4% interval ratio is nearly trapezoidal with a flat top over 60 degrees. However, the experimental EMF waveform is sinusoidal, which means that the winding coil is well distributed in the stator.

Table 1 Rating of mechanical parameters of the motor

Output power	300 W
Rated torque	5.6 Nm
Rated speed	510 rpm
Total weight	3.5 kg
Torque/total weight ratio	1.6 Nm/kg
Inner rotor radius, R_i	62 mm
Outer rotor radius, R_o	104 mm
Mid. Radius, R_{md}	80 mm
Rep. Radius, R_{rp}	85 mm
Pole pitch in circle of R_{rp}	27 mm
Transversal length	23 mm
Magnet thickness, l_m	3 mm
Airgap length, l_g	13 mm
Coefficient of flux distribution, k_ϕ	0.85

Table 2 Rating of electrical parameter of the motor

Rated Current, I_{dc}	10.3A
Rated Current, I_{ph}	8.4A
Rated Voltage, V_{dc}	36V
Number of phases, m	3
Number of poles, p	20
Number of magnets	2×20
Resistance per phase	0.23 Ω
Air gap flux density, B_g	0.38 T
Number of total coils	60
Turns per coil	16
Number of parallel circuits	2
Conductor diameter	2×ϕ0.8 mm

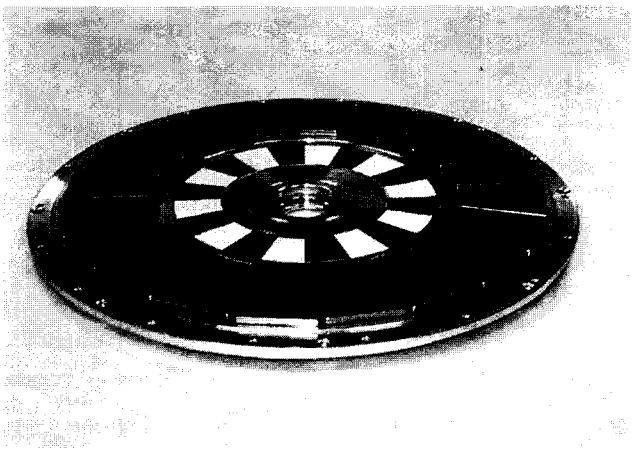

Fig. 7 Prototype AFPM coreless motor: Rotor

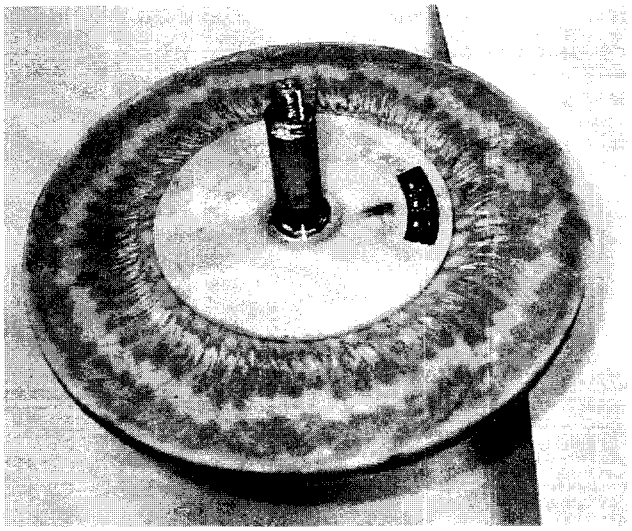

Fig. 8 Prototype AFPM coreless motor: Stator

The instantaneous torque per phase can be computed from the load current and back EMF of Fig. 9 using the position signals to tie the two sets of waveforms together. One phase and total torque are shown in Fig. 10. The waveform of total torque is obtained by adding the waveforms of each phase torque, which are 120° offset electri-

cally. The ideal waveform of the torque from the sinusoidal EMF and piecewise constant load current makes torque ripple inherently. The experimental waveform of torque has more torque ripple due to the current spike of the commutation process, which must be reduced, but is less severe when compared with [13]. Torque ripple is absorbed by the inertia of the rotor and wheel and makes small electrical noise.

Fig. 11 shows the load test bench of the motor, and Fig. 12 illustrates the results of the load test. As a result, the efficiency of the motor at the rated output approaches 85%, which is very a high efficiency compared with other motors in this low-speed range. An induction motor in this speed range must have 14 poles in the rotor, and its efficiency is about 60%. The manufactured prototype of our motor has a rating of 300W, 510rpm and 5.6Nm. These figures are sufficient for our electric scooter application and are shown as proper characteristics for such kind of load demands. Fig. 13 shows the electric scooter equipped with this prototype AFPM coreless motor. Compared to other similar research results [14], this motor has better efficiency and output.

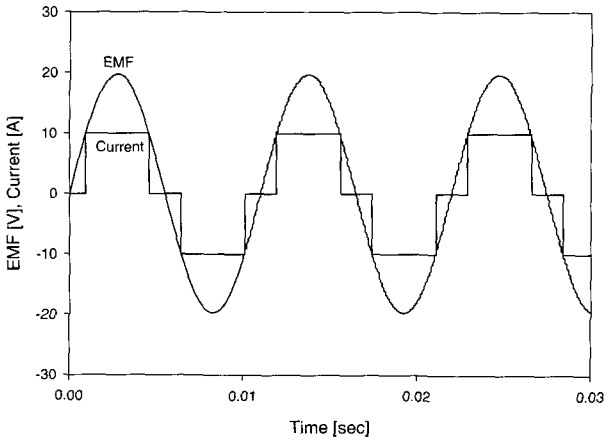

a) Ideal waveforms

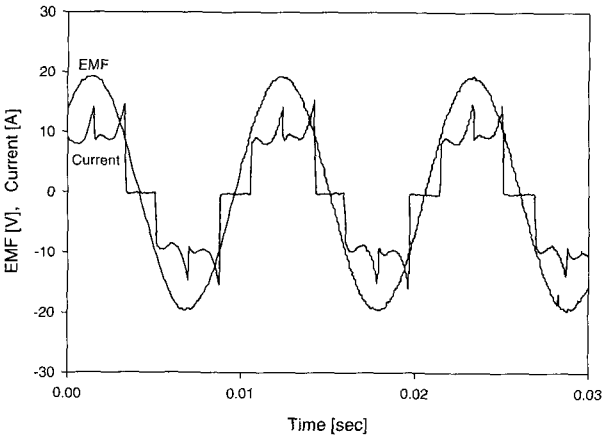

b) Experiment waveforms

Fig. 9 Phase EMF and load current at the rated speed

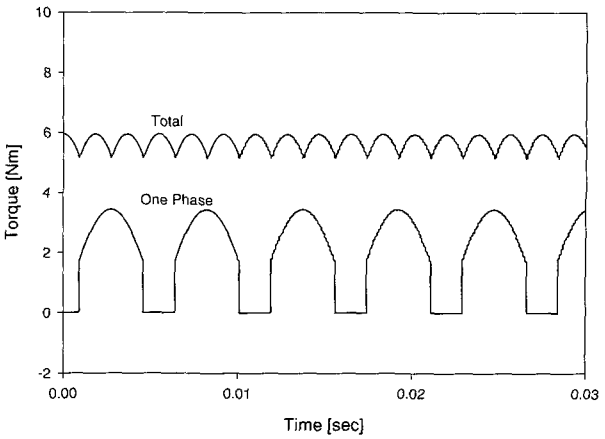

a) Ideal waveforms

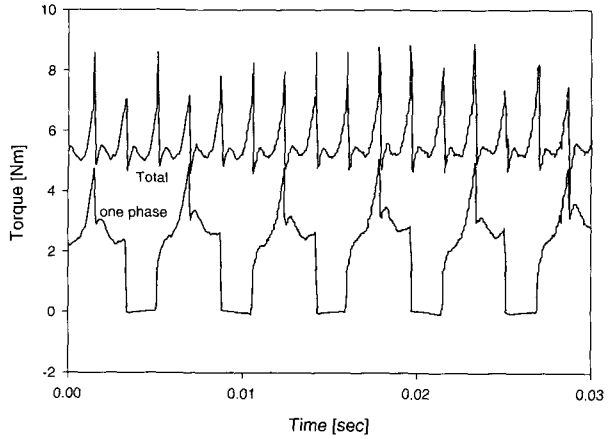

b) Experiment waveforms

Fig 10. Instantaneous electrical torque

Fig. 11 Load test bench of the motor

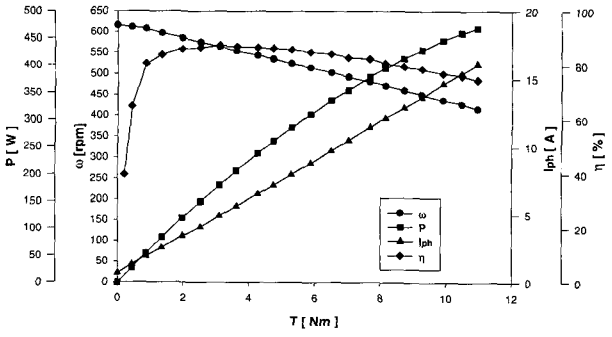

Fig. 12 Characteristics of the prototype AFPM coreless motor

Fig. 13 Electric scooter of the prototype AFPM coreless motor

3. Conclusion

In this paper, design and analysis of the prototype coreless AFPM motor in the 300W power range were researched and a characteristic equation is derived from both methods, the Lorentz force law and the energy conversion law. The torque equation was verified through practical calculation. To determine the leakage effect of the magnetic flux at the airgap, the interval ratio of the permanent magnets was introduced. FEM simulation was carried out to find the proper interval ratio, and a 4% interval ratio was chosen for the prototype motor.

A prototype of this AFPM motor was manufactured and applied to the electric scooter, which requires a low-speed, high-torque motor. Tests of this AFPM motor on the load test bench as well as applied to powering an electric scooter have shown satisfying results.

References

[1] F. Caricchi, et al, "Low-Cost Compact Permanent Magnet Machine for Adjustable-Speed Pump Applica-tion," *IEEE Transactions on Industry Applications*, Vol. 34, No. 1, pp. 109-116, 1998.

[2] K. Sitapati and R. Krishnan, "Performance Comparisons of Radial and Axial Field, Permanent Magnet , Brushless Machines," *IEEE Transactions on Industry Applications*, Vol. 37, No. 5, pp. 1219-1226, 2001.

[3] Z. Zhang, et al., "Wheels Axial Flux Machines for Electric Vehicle Applications," *International Conference on Electrical Machines*, pp. 7-12, 1994.

[4] E. Spooner and B.J. Chalmers, "TORUS: a Slotless, Toroidal-Stator, Permanent-Magnet Generator," *IEE Proceedings-B*, Vol. 139, No. 6, pp. 497-506, 1992.

[5] T.A. Lipo, "A Low-Loss Permanent-Magnet Brushless DC Motor Utilizing Tape Wound Amorphous Iron," *IEEE Transactions on Industry Application*, Vol. 28, No. 3, pp. 646-651, 1992.

[6] F. Profumo, et al, "Design and Realization of a Novel Axial Flux Interior PM Synchronous Motor for Wheel-Motors Applications," *Electric Machines and Power Systems*, Vol. 28, pp. 637-649, 2000.

[7] Yurity N. Zhilichev, "Three-Dimensional Analytic Model of Permanent Magnet Axial Flux Machine," *IEEE Transactions on Magnetics*, Vol. 34, No. 6, pp. 3897- 3901, 1998.

[8] B. J. Chalmers, W. Wu, and E. Spooner, "An Axial-Flux Permanent-Magnet Generator for a Gearless Wind Energy System," *IEEE Transactions on Energy Conver-sion*, Vol. 14, No. 2, pp. 251-257, 1999.

[9] T.S. El-Hasan, P.C. Luk, F.S. Bhinder, and M.S. Ebaid, "Modular Design of High-Speed Permanent Magnet Axial-Flux Generators," *IEEE Transactions on Magnet-ics*, Vol. 36, No. 5, pp. 3558-3561, 2000.

[10] P. Campbell, *Permanent Magnet Materials and their Application*, Cambridge University Press, 1994.

[11] Duane C. Hanselman, *Brushless Permanent-Magnet Motor Design*, McGraw-Hill, pp. 41-60, 1994.

[12] H. Chai, *Electromechanical Motion Devices*, Prentice Hall, 1998.

[13] A. G. Jack, et al, "Combined Radial and Axial Permanent Magnet Motors Using Soft Magnetic Composites," *IEE Ninth International Conference on Electric Machines and Drives*, pp. 25-29, 1999.

[14] T. F. Chan, et al, "In-Wheel Permanent-Magnet Brushless dc Motor Drive for an Electric Bicycle," *IEEE Transactions on Energy Conversion*, Vol. 17, No. 2, pp. 229-233, 2002.

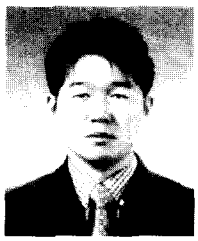

Chul-Ho Kim
received the B.S. degree from Kyungil University and M.S. degree from Kyungpook N. University in 1995 and 1997, respectively. He is currently working toward the Ph.D. degree at Kyungpook N. University. His research fields are design of permanent magnet motors and wind power generating systems.

Chul-Soo Oh
received the M.S. degree from Technical University Stuttgart in Germany in 1966, and the Ph.D. degree from Yeungnam University in 1989. He has been with Kyungpook N. University, Daegu, Korea, since 1984. His research interests are power engineering, motor design, and wind power system engineering.